

## EFFECT OF COILING TEMPERATURE ON THE STRUCTURE AND PROPERTIES OF THERMO-MECHANICALLY ROLLED S700MC STEEL

S. Oktay <sup>a</sup>, P.E. Di Nunzio <sup>b\*</sup>, M.C. Cesile <sup>b</sup>, K. Davut <sup>c</sup>, M.K. Şeşen <sup>d</sup>

<sup>a</sup> Istanbul Technical University, Istanbul, Turkey

<sup>b</sup> RINA Consulting – Centro Sviluppo Materiali S.p.A., Rome, Italy

<sup>c</sup> Department of Materials Science and Engineering, İzmir Institute of Technology, İzmir, Turkey

<sup>d</sup> Istanbul Technical University, Istanbul, Turkey

(Received 04 March 2022; accepted 13 October 2022)

### Abstract

The boron-free S700MC steel is usually produced by exploiting the properties of a ferrite-bainite mixed microstructure formed by coiling the strips at a temperature of about 450°C, i.e. below the bainite starting temperature. With the aim of further enhancing the mechanical properties of 6 to 10 mm thick strips, industrial tests were carried out at a coiling temperature of 600°C to promote the formation of a structure of ferrite and carbides, which is also acceptable for this type of steel. Unexpectedly, a microstructure composed of ferrite and martensite was obtained. Compared to the ferritic-bainitic grade, the new structure is characterized by a slight decrease of the yield point but by an increase of the ultimate tensile strength by no less than 80 MPa, with a transition from a quasi-discontinuous to a clearly continuous yielding behaviour. Accordingly, the ratio of yield strength to tensile strength decreases from 0.90 to 0.75 and the impact energy decreases by 35 J and 60 J for the two gauge levels, respectively.

The mechanical behaviour of the strips coiled at high temperature is explained as a direct consequence of the dual phase structure with a hard phase interspersed in a soft ferrite matrix. The presence of martensite is explained by the so-called incomplete bainite reaction. The partial transformation into ferrite after coiling and the long time required for the coil to cool down stabilize the untransformed austenite due to the carbon enrichment making bainite formation at lower temperatures impossible.

**Keywords:** HSLA steels; Phase transformation; Microstructure; EBSD technique; Mechanical properties

### 1. Introduction

Microstructure and mechanical properties of high strength steels (HSS) are determined by the combined effect of chemical composition and thermomechanical processing (TMP). An essential contribution in increasing the mechanical properties comes from the addition of precipitate-forming elements, such as Ti, Nb, or V. Among them, niobium plays a central role in refining the austenite microstructure during hot rolling because it retards austenite recrystallization through grain boundary pinning by high-temperature strain-induced precipitation. Low-temperature precipitation provides a further strengthening of the ferrite matrix thus enhancing the work hardening of the final product.

The automotive industry is interested in the continuous improvement of the performance of flat rolled sheets which combine a high strength with an adequate elongation to reduce vehicle weight and

increase the fuel efficiency. Among the different grades, HSS have a high tensile strength and both an acceptable elongation and excellent hole expansion performance which ensures a good formability [1]. In particular, the S700MC grade offers a good combination of strength and toughness that makes it the best choice whenever wear resistance is required together with good formability. This grade is ideal for structural applications in the automotive industry as shown by Mesplont et al. [2] and more recently also by Bian et al. [3], and for components related to passenger safety such as anti-intrusion frames. This grade is also suitable for road restraint systems when a very high containment level is requested [4].

From the metallurgical viewpoint, the 700 MPa yield strength grade can be achieved by a twofold strategy. The first one relies on a specific alloy design (less than 0.1 wt% carbon, about 2 wt% Mn and Nb, Mo, Cr, V). The second one, with a leaner chemical composition, exploits the properties of boron in

\* Corresponding author: paolo.dinunzio@rina.org



amounts of the order of 20 to 30 parts per million in mass to retard the ferrite formation during cooling thus promoting bainitic structures.

The boron-free S700MC is widely studied in the literature for different aspects related to the industrial processing route for exploiting its high flexibility in controlling the final microstructure. An example is the use of ausforming and tempforming [5, 6] for obtaining a structure of tempered martensite or very refined ferrite to improve toughness.

One of the main issues of this material is related to the stability of its microstructure during thermal treatments. The fine-grained microstructure, especially if it also contains bainite, is quite unstable when subjected to thermal treatments or thermal cycles. In fact, if temperature is high enough, it can change its precipitation state and promote recrystallization [7]. Depending on the steel's chemical composition, this could lead to an increase in mechanical properties for temperatures and times typical of tempering treatments, i.e. in the range of 600 to about 700°C [8]. On the other hand, if temperatures are even higher, as for example in case of fire, strength is reduced which can lead to failure in structural components [9].

Another fundamental aspect for the final application of this steel is welding. As a matter of fact, due to the high intrinsic hardenability of this grade, undesired hard microstructures can easily be obtained in the heat affected zone (HAZ) of welded joints, especially when not enough attention is paid to the operating procedures [10]. A rigorous control of the heat input, together with a proper welding technique (for example MAG [11]) are mandatory to limit the austenite grain coarsening in the HAZ [12]. This would also promote the formation of bainite and martensite, and also reduce residual stresses [13].

This work is focused on the S700MC grade obtained by alloys of the first type [14] which exhibit a remarkable robustness against temperature variations on the run-out table of the hot-strip mill. At the same time, besides the effect of alloying elements [15,16], the steel microstructure is controlled by the hot rolling processing conditions and, in particular, by the coiling temperature (CT) of the strip. Generally speaking, for the S700MC grade, high coiling temperatures promote the formation of a fine-grained polygonal ferrite with precipitation strengthening, whereas for low coiling temperatures below the bainite start (Bs) temperature, a microstructure composed of a mixture of ferrite and bainite is obtained. In the latter case, a higher hardenability, which is obtained by higher alloying of Mn, Mo and Cr, is needed. Higher hardenability is required especially for strips thicker than about 5 mm, due to the unavoidable limitations in achieving cooling rates on the run-out table (ROT) of the hot rolling mill.

Cooling rates should be high enough to form bainite and to ensure the best homogeneity of the microstructure through the strip thickness.

A fine microstructure is mandatory, especially regarding the ferrite fraction of the structure, since it contributes with an additional strengthening effect. To this purpose, the grain refining effect of Nb has to be fully exploited by controlling the austenite non-recrystallization temperature of the steel and the hot rolling schedule [17,18].

Both structures, ferrite-carbides and ferrite-bainite, are known to produce similar yield and tensile strength [14]. In general, the fully ferritic microstructures have higher elongation while the ferrite-bainite microstructures exhibit a better toughness.

The present study has been carried out on a boron-free S700MC steel grade, which is produced according to the current industrial practice involving a coiling temperature of 450°C. This temperature is below the bainite start temperature and ensures obtaining a microstructure composed of a mixture of ferrite and bainite. Following the suggestions from the abovementioned work [8] indicating that an increase in the mechanical properties could be achieved by a tempering treatment of the as hot rolled strip at 600°C, an attempt has been made to coil strips of thickness greater than approximately 5 mm directly to this temperature. The aim was to exploit the precipitation hardening capabilities of the alloy by developing a ferrite-carbides structure in the coil. The CT was selected not higher than 600°C to avoid issues related to the known high hardenability of the steel. However, unexpectedly, by processing strips of 6 mm and 10 mm thickness with the high-CT route, a microstructure of ferrite and martensite was obtained.

The aim of this study is to understand the metallurgical mechanisms responsible for such a finding. As a matter of fact, although the rich chemical composition of the industrial formulation here considered has been purposely developed for ensuring the adequate hardenability for thick gauge strips, the presence of martensite instead of carbides or even bainite, demands to be analysed and discussed with a specific focus on its technological consequences, since this structure undoubtedly exhibits an interesting mechanical behaviour.

## 2. Materials and methods

Strips of S700MC steel grade were industrially hot rolled to a thickness of 6 and 10 mm and each one coiled at low (450-480°C) and high (600°C) temperature. The chemical composition of the steel was determined via ARL 4460-978 optical emission spectroscope, and complies with the DIN EN 10149 2. Its main features are summarized in Tab. 1. The



coiling temperatures and the corresponding sample codes are listed in Tab. 2. In all cases the hot rolling has been finished above the  $A_{e3}$  temperature. It is worth noticing that no boron is added to the steel chemical composition to enhance its hardenability. Consequently, the austenite transformation kinetics towards a bainitic structure is controlled mainly by the amount of Mn, Cr and Mo and by the cooling strategy on the run-out table of the hot rolling mill.

**Table 1.** Chemical composition of the hot rolled strip (mass %)

Strips	C	Mn	Si	N	Al	Cr+Mo	Nb	Ti+V
S1-S2	0.09	2.0	0.20	0.006	0.045	<0.7	0.080	<0.2
S3-S4	0.07	1.9	0.17	0.006	0.044	<0.7	0.075	<0.2

**Table 2.** Coiling temperature and thickness of the hot rolled strips

	S1	S2	S3	S4
Coiling temperature, CT (°C)	450	600	480	600
Strip thickness (mm)	6	6	10	10

The microstructure of the samples was examined by optical microscope (OM) and scanning electron microscope (SEM). The strips were prepared for metallographic examination on longitudinal sections containing the rolling direction (RD) and the normal direction (ND). Specimens were sectioned via an abrasive cut-off machine, grinded with SiC papers and then polished with diamond paste down to 1  $\mu\text{m}$  by a fully automated grinding/polishing machine. Afterwards, the specimens were etched with 4% Nital solution. Micrographs of the sections were taken by an optical microscope, at magnifications from 50x to 500x under bright field illumination. The SEM micrographs were taken by a Merlin field-emission gun (FEG) SEM using the secondary electron detector. Additionally, the electron back-scatter diffraction (EBSD) technique was employed to analyse in detail the crystallographic features of the microstructures, e.g., grain and sub-grain structure, grain boundary character, misorientations. For the EBSD analysis, a Zeiss Merlin FEG-SEM equipped with EDAX/TSL EBSD system and a Hikari EBSD camera was used, with an accelerating voltage of 15 kV, a beam current of 6.0 nA and a working distance of 13 mm. EBSD maps were measured on a of 80 x 80  $\mu\text{m}$  area with a step size of 50 nm on a hexagonal grid. The EBSD camera was run at 100 frames per second with 15 ms exposure time in 4x4 binning (160x120 pixels). During the post-processing of the raw EBSD data, firstly the grain confidence index standardization (GCIS) method was used to check the confidence index (CI) of all points within a grain and then the highest found value to all points in that grain

was assigned. Afterwards, a minimum CI-filter of 0.1 was used to exclude only the certainly falsely indexed points. It has to be noticed that the clean-up procedure does not change the measured orientation of any point.

Tensile tests were carried out on samples taken parallel to the longitudinal direction. Charpy V notch impact tests were performed at temperatures of -20°C and -40°C on test specimens taken parallel the longitudinal direction as well, having size 10x5x55 mm for 6 mm thick strips and 10x7.5x55 mm for 10 mm thick strips. Three specimens for each mechanical test and per testing temperature were used.

X-ray diffraction measurements were performed by a Siemens D500 goniometer in Bragg-Brentano geometry using the  $\text{Co-}\alpha$  radiation. The determination of the retained austenite was carried out by a Rietveld full-pattern refinement using the commercial software Match! by Crystal Impact (<http://www.crystalimpact.com/match/>) in the 2 $\theta$  range from 45 to 105 degrees.

### 3. Results

#### 3.1. Microstructural analysis

The images taken by optical microscope are shown in Fig. 1. In all cases the prior heavily deformed austenite structure, composed of bands parallel to the rolling direction, is quite apparent. All the structures are very refined with a mean grain size of about 2  $\mu\text{m}$ , i.e., of the same order of the prior austenite band thickness. In samples S2 and S4 some coarsening of ferrite grains is observed. A more detailed examination has been carried out by SEM and the most significant images are reported in Fig. 2. Particles of Nb-Ti carbonitrides of average size between 80 and 250 nm, have been observed by SEM in all specimens.

The microstructure of samples S1 and S3 appear composed of a mixture of upper bainite and ferrite. In higher magnification SEM pictures, the inter-lath precipitation of cementite is clearly visible. In the optical micrographs of the strip S1 some regions characterized by large and elongated ferrite grains with a subgrain structure (and probably also a high dislocation density) can be observed.

Samples S2 and S4 have a ferritic structure with interspersed martensite islands of 2 to 5  $\mu\text{m}$  and 1 to 2  $\mu\text{m}$  average size, respectively. The second phase appears grey in the optical images at low magnification and exhibits its typical substructure in the SEM pictures taken at higher magnification.

A quantitative evaluation of the microstructural constituents is difficult due to the substantial similarity between upper bainite and (non-polygonal) ferrite. In the approximate measurements carried out manually by point counting, the grains having a more



equiaxed shape and neither apparent sub-grain structure nor inter-lath cementite precipitation have been assumed to be ferrite, the remaining structure being classified as upper bainite. In specimens S2 and S4, only ferrite and martensite have been considered and, in this case, the quantitative evaluation has been straightforward. The x-ray diffraction analysis carried out on all the specimens has revealed that in strip S3 only there is about 4 vol% of retained austenite, which suggests the formation of some granular bainite together with upper bainite. A summary of the measured volume fractions is reported in Tab. 3.

**Table 3.** Quantitative evaluation of the microstructural constituents in the studied specimens (vol.%). Retained austenite has been determined by x-ray diffraction

	S1	S2	S3	S4
Bainite	56±5	traces	38±5	Traces
Martensite	0	35±5	traces	20±5
Ferrite	44±5	65±5	58±5	80±5
Retained Austenite	0	0	4	0

### 3.2. Mechanical properties and impact testing

The results of the tensile and impact tests are summarized in Table 4. It is worth giving the tensile properties of steel grade S700MC according to the reference standard DIN EN 10149-2, in order to compare them with the properties of the specimens. The reference values are as follows:  $R_{eH}$  not less than 700 MPa (not less than 680 MPa for thickness of 8 mm or more),  $R_m$  from 750 to 950 MPa and elongation not less than 12%.

Both yield strength and ultimate tensile strength are higher in the S1 and S2 strips compared to the corresponding ones S3 and S4. This is primarily due to the higher content of C and Mn in the former strips. Moreover, it is also a consequence of the smaller thickness which favours a more homogeneous microstructure between sub surfaces and central region of the strip with a higher fraction of hard constituents (bainite in S1 and martensite in S2).

For both thickness levels, the  $R_{p0.2}$  of strips coiled at higher temperature is slightly lower than that of the corresponding one coiled at lower temperature. Conversely, the  $R_m$  is markedly higher (not less than 80 MPa) in the strips coiled at higher temperature.

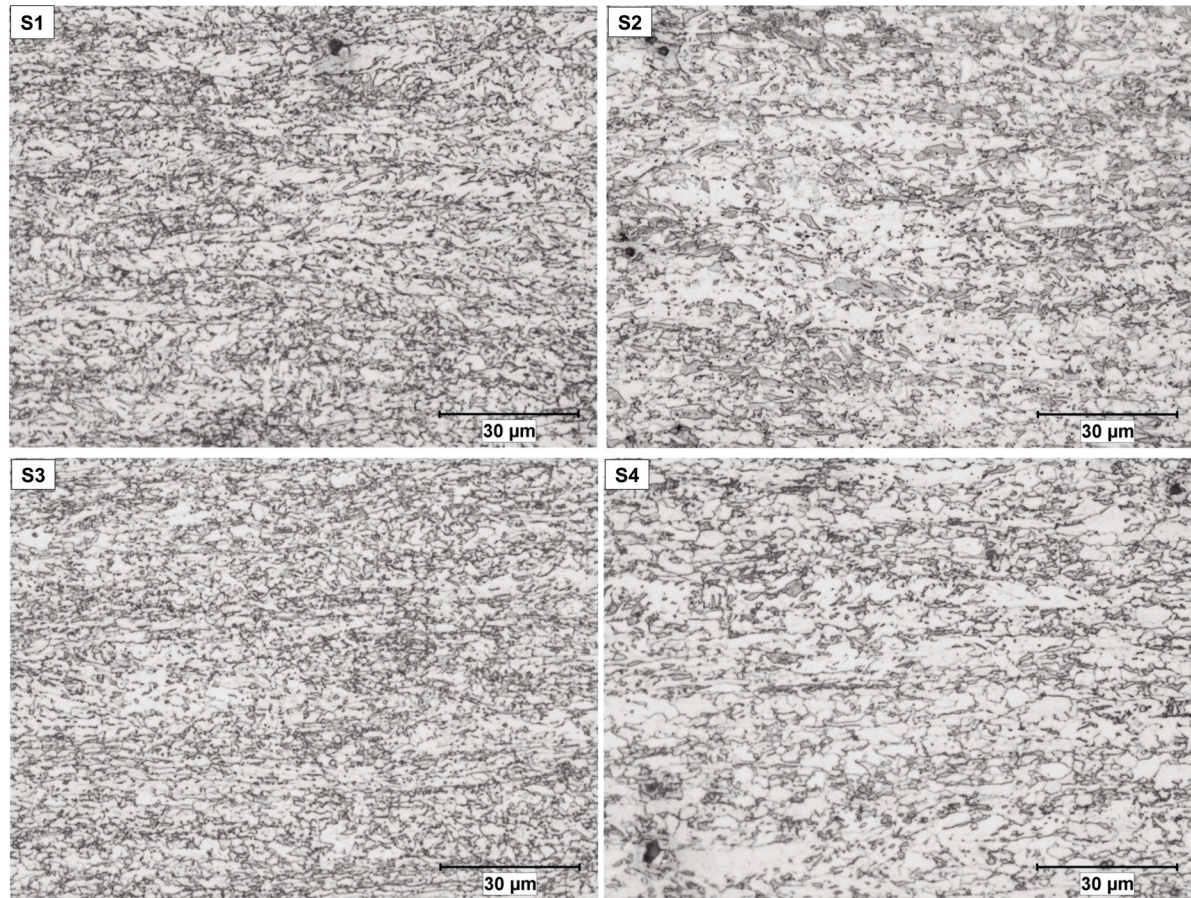


**Figure 1.** Microstructures of S700MC steel at mid thickness (optical microscope, 4% Nital etching)

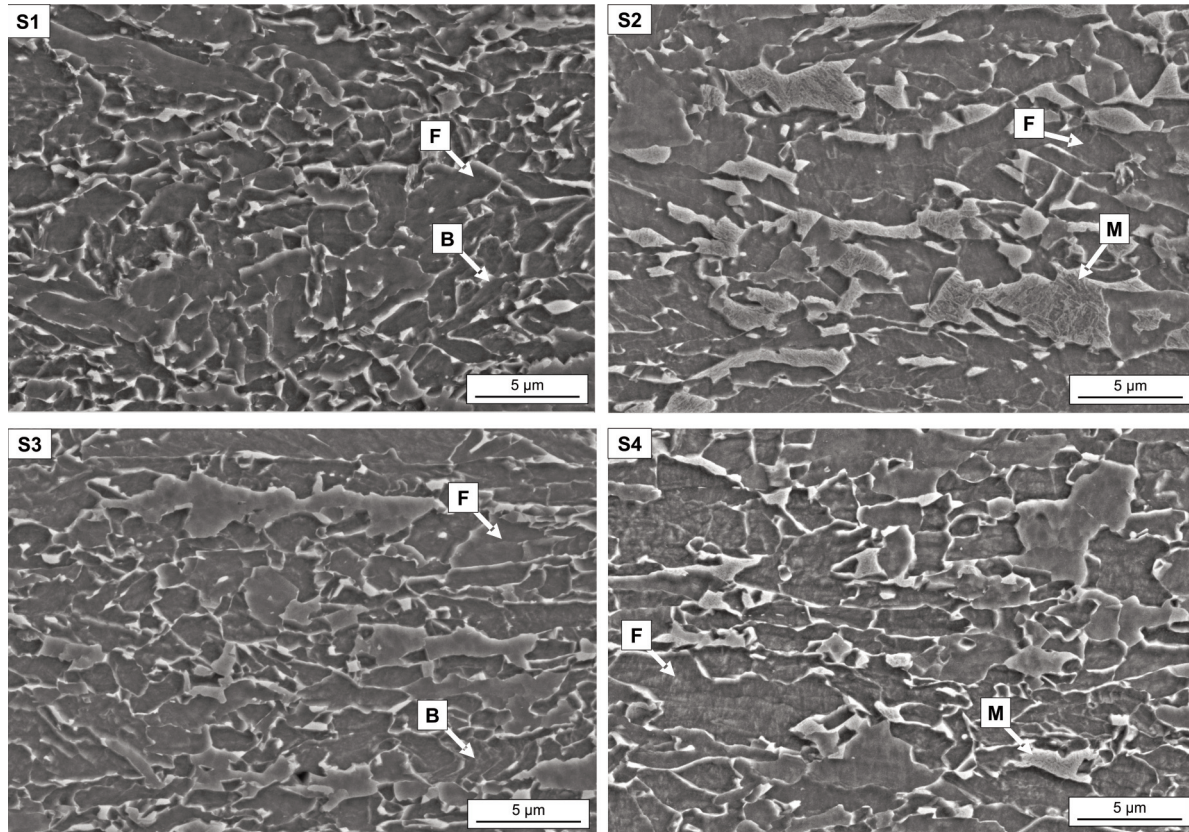


**Figure 2.** SEM micrographs of the studied samples at mid thickness (SE, 10 kX). Legend: F=Ferrite, B=Bainite, M=Martensite

The elongation slightly increases with increasing the coiling temperature and, as expected, with the strip thickness. The stress-strain curves of the specimens are shown in Fig. 3. It can be observed that the strips coiled at higher temperature have a clearly continuous yielding, whereas those coiled at lower temperature show a moderate discontinuity with no clear upper yield point but some Lüders elongation regime, especially in S3. Together with the parallel relevant decrease of the  $R_{p0.2}$  to  $R_m$  ratio from about 0.90 (low CT) to about 0.75 (high CT), this confirms the presence of bainite as major constituent in the strips coiled at low temperature.

Charpy V notch impact tests show that the samples

S1 and S3 with lower CT have a higher impact energy at both the test temperatures than samples S2 and S4. The drop of impact energy is about 60 J from S1 to S2 and slightly lower from S3 to S4 (ranging from 35 to 50 J). Also in this case, the presence of bainite in S1 and S3 is confirmed since higher impact energies are associated to a different distribution of grain misorientation. This aspect will be discussed later with EBSD results.

### 3.3. Bending Tests

Bending tests were carried out on the thicker gauge strips only with test samples transverse to the

**Table 4.** Tensile properties and impact energies of the S700MC strips

	S1	S2	S3	S4
	6 mm low CT	6 mm high CT	10 mm low CT	10 mm high CT
$R_{p0.2}$ (MPa)	730±1.5	732±2.0	679±2.0	681±1.0
$R_m$ (MPa)	816±1.5	981±0.5	776±5.0	855±2.0
Total elongation (%)	15.1	15.5	16.4	18.6
$R_{p0.2}/R_m$	0.89	0.75	0.88	0.80
Impact energy @-20°C (J)	128±4.9	67±2.5	139±13.7	88±6.9
Impact energy @-40°C (J)	120±7.5	60±4.3	110±6.8	75±5.6

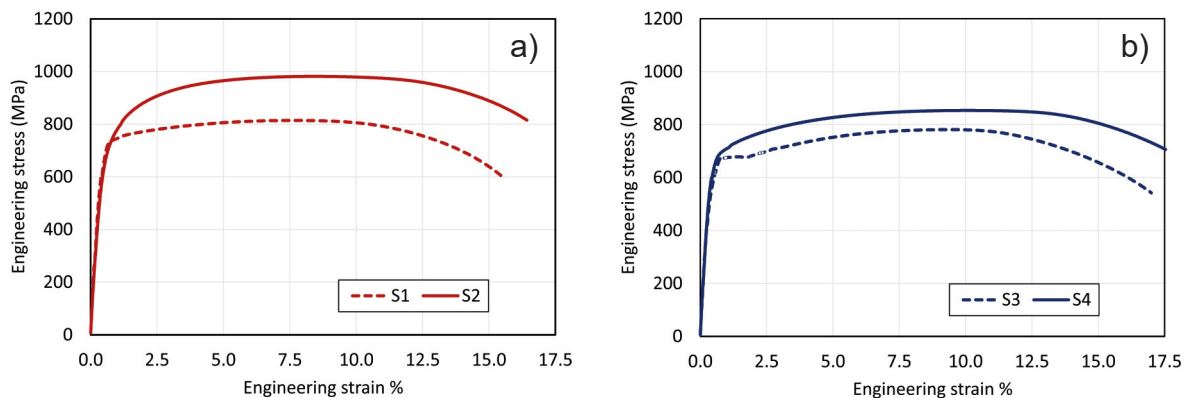


Figure 3. Stress-strain curves of a) S1 and S2 (6 mm thickness) and b) S3 and S4 (10 mm thickness)



Figure 4. Side and top view of the bent specimens of 10 mm thick S3 (a) and S4 (b) strips

rolling direction using a mandrel with a diameter of 10 mm. The images of bent samples, reported in Fig. 4, show defect-free surfaces in both the low CT strip S3 and in the high CT strip S4 notwithstanding the difference in microstructure.

#### 4. Discussion

There are two main issues, strictly related to one another, that deserve to be discussed in detail. The first one is the difference in yielding behaviour of the strips as a function of the coiling temperature, the second one is the reason why martensite is found in strips coiled at high temperature after a slow cooling.

Regarding the difference in yielding and the relevant increase in strength induced by a high coiling temperature, it is apparent that the deformation behaviour of strips S2 and S4 is typical of a microstructure composed of a soft matrix phase (ferrite) with an interspersed hard phase (martensite). Although it has been obtained with a different thermal treatment and chemical composition, this microstructure is similar to that exploited by Tasan et al. [19] in dual phase (DP) steels to achieve a high strain hardening, especially at the beginning of plastic deformation. The main difference is that in DP steels the martensite has a higher carbon content.

The transition from a discontinuous to continuous yield point is a common finding in similar steels in the literature, even if bainitic microstructures are involved.

Graux et al. [20] studied a steel with 0.06% C, 1.9% Mn, 0.5% Si, 0.1% Ti, 0.04% Nb, 0.2% Mo, 0.03% Cr, 0.05% Al, 0.005% N where granular bainite is found at relatively small cooling rates, approximately less than 5°C/s. It is associated to mixed microstructures where ferrite is formed at higher temperature and the untransformed austenite is enriched in carbon. The high Si content, in conjunction with the presence of Mo as hardenability promoter, suppresses the precipitation of cementite favouring the formation of the carbide-free granular bainite. As the cooling rate increases the structure shifts towards a lath-like upper bainite.

In this respect, as already pointed out, the presence of a small amount of retained austenite in strip S3 is reasonably associated to granular bainite. This constituent is found in S3 and not in S1 because the former has been coiled at a temperature about 30°C higher than the latter (Tab. 2).

As pointed out by Bhadeshia [21] and also by Josefsson and Andr n [22], granular bainite is a form of bainite that occurs during continuous cooling transformations or non-isothermal heat treatments,

whose characteristic features are coarse sheaves of bainitic ferrite and the lack of carbides in the microstructure. Instead, the carbon partitioned from the bainitic ferrite stabilises the residual austenite, so that the final microstructure contains both retained austenite and some high carbon martensite in addition to the bainitic ferrite.

A more significant comparison is found in the work by Mesplont et al. [2], that focusses on the development of hot-rolled, formable high-strength bainitic steels for automotive applications where the relationship between microstructure and mechanical properties is studied in connection with chemical composition and processing conditions. The steels considered have a chemical composition similar to that of S700MC, but with a higher carbon and silicon content. In the average, those steels contain 0.16% C, 1.6% Mn, 0.26% Si, 0.45% Cr, 0.2% Mo, 0.05% Nb, 0.024% Ti and 20 ppm B to promote the formation of a bainitic structure.

In particular, the authors exploit an increase in the coiling temperature to shift from a predominantly bainitic microstructure, with high yield strength and high yield-to-tensile ratio, to a duplex bainite-austenite microstructure with high tensile strength and low yield-to-tensile ratio, which ensures an improved formability. The isothermal transformation from deformed austenite has been studied in detail revealing that it produces a mixture of bainite and retained austenite. This treatment is somehow analogous to coiling at high temperature as in the case of strips S2 and S4, since the slow cooling rate of the industrial coil (about 20°C/h) ensures a quasi-isothermal holding at a temperature close to 600°C for a long time. Moreover, the behaviour of the yield-to-tensile ratio is exactly the same observed in the S700MC strips.

#### 4.1. Analysis of the transformation mechanism

The analysis of the results on S700MC can now be attempted starting from the evaluation of the average cooling rate imposed to the strips on the run-out table considering the length of the cooling zone, the target coiling temperature, and the strip velocity. On one hand, this helps to quantitatively ascertain the general behaviour of the material during cooling and, on the other hand, it provides an indirect validation of the metallurgical models that are employed in the following discussion.

According to the operating practices adopted in the industrial production of the S700MC grade, the average cooling rates in the ROT section where the cooling system was active have been estimated as 55, 35, 34, and 21°C/s for S1, S2, S3, and S4, respectively. It can be observed that strips S2 (6 mm, high CT) and S3 (10 mm, low CT) have a similar

average cooling rate at least in the first stage of cooling, although their coiling temperatures are different, and consequently more ferrite is expected to form in S2.

The no-recrystallization temperature of the steel has been calculated according to the Boratto's empirical relationship [23]:

$$T_{nr} (^{\circ}\text{C}) = 887 + 464 \cdot \text{C}\% + (6445 \cdot \text{Nb}\% - 644 \cdot \sqrt{\text{Nb}\%}) + (732 \cdot \text{V}\% - 230 \cdot \sqrt{\text{V}\%}) + 890 \cdot \text{Ti}\% + 363 \cdot \text{Al}\% - 357 \cdot \text{Si}\% \quad (1)$$

For this steel it is greater than 1100°C, a high value but not unusual for highly microalloyed grades. It ensures that, even for hot rolled strips with relatively large thickness, as those here considered, a fully pancaked structure and a relevant strain accumulation are obtained during the hot rolling finishing stage. As a matter of fact, traces of the prior banded austenite microstructure are clearly visible in the optical micrographs in Fig. 1 as well as in the SEM images in Fig. 2. The thickness of prior deformed austenite grains can be estimated roughly in the range between 1 to 3 μm.

The standard coiling conditions for the S700MC grade, namely a coiling temperature of 450°C, have been defined based on the steel chemical composition and austenite grain size by estimating a bainite start temperature of about 485°C.

A graphical representation in terms of a paraequilibrium CCT diagram calculated according to ref. [24] assuming the last finishing pass at 870°C with 30% hot deformation and a mean austenite grain size of 2 μm is reported in Fig. 5. The modelling approach adopted, which is applicable to low- and medium-alloyed steels, has been fully developed in-house. It is composed by a thermodynamic module and by a kinetic module. The former can be used separately to calculate simple phase equilibria, involving only austenite and ferrite, in multicomponent systems. The thermodynamic part is based on the CALPHAD method and evaluates the molar Gibbs free energies of austenite and ferrite as a function of temperature and chemical composition. The minimization of the overall energy of the system is carried out imposing the equilibrium condition defined by equating the chemical potential of all the components in both phases, which is equivalent to find the common tangent to the free energy surfaces in the multi-dimensional composition space. The thermodynamic database used for the calculations was extracted from that associated to *MatCalc* package (version 5.42, database mc\_fe\_v2.017.tdb), a commercial scientific software toolbox for computer simulation of constrained and unconstrained phase equilibria and precipitation kinetics [25].

In the paraequilibrium condition, only the carbon



partitioning is allowed between austenite and ferrite, while all the substitutional elements retain their nominal composition. Therefore, by constraining the equilibrium condition of equal chemical potential of carbon in both phases, the phase diagram shown in Fig. 6 can be calculated. The description of the transformation kinetics according to the paraequilibrium assumption is justified whenever the austenite decomposition takes place as a consequence of relatively fast cooling rates, such as those here imposed on the run-out table of a hot strip mill. In such conditions, the thermodynamic driving force for phase transformation is not maximized but the overall kinetics is faster.

The CCT diagram in Fig 5 is evaluated by the joint use of thermodynamic and kinetic modules. The austenite decomposition kinetics are modelled starting from the driving force for the transformation which is calculated using the thermodynamic module. This allows the calculation of the nucleation rate of ferrite, pearlite, and bainite along the austenite grain boundaries based on the knowledge of the mean austenite grain size, the residual strain due to austenite deformation and the given cooling profile. Once the nuclei are formed, the microstructural constituents can grow. Ferrite and pearlite transformations are reconstructive in nature and therefore the growth of these constituents is controlled by carbon diffusion in austenite [26]. For bainite, a displacive (partition-free) model was intentionally developed, in which nucleation of primary and secondary units of bainitic ferrite occurs sequentially but is described by two different kinetic equations without considering autocatalytic effects.

Finally, if some austenite is still present at the  $M_s$  temperature, it transforms to martensite according to the Koistinen and Marburger equation [27]. The whole model has been calibrated on a set of CCT diagrams partly taken from the literature and partly from an internal archive.

The continuous cooling curves shown in Fig. 5 were stopped at their respective coiling temperatures and switched to isothermal holdings just to illustrate the actual average thermal path. It can be observed that the bainitic structure can be achieved in the strips coiled at low temperature although it is possible that some ferrite could form at mid thickness. Similarly, when coiling temperature is high, ferrite starts forming when the strip is at ROT but, as mentioned earlier, the phase transformation is probably not complete until after coiling since bainite cannot form at a temperature above  $B_s$ . Moreover, the coiled strip cools down slowly (about 15 to 20°C/h) allowing sufficient time not only for the interstitial carbon precipitated from the ferrite to be distributed uniformly throughout the austenite, but possibly also for an at least partial distribution of the substitutional

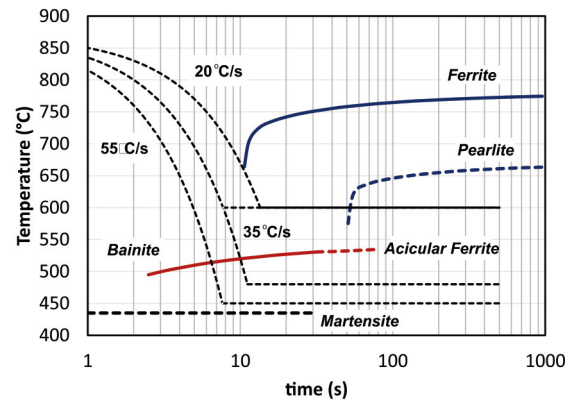


**Figure 5.** Calculated CCT diagram for the S700MC steel (average composition) assuming austenite deformed 30% at 870°C with a mean grain size of 2  $\mu\text{m}$  and paraequilibrium conditions. Curves refer to 5 vol.% transformation

elements, especially Mn, so that the stability of the austenite is further increased. Roughly speaking, the time required for a strip coiled at 600°C to cool to 400°C, a temperature low enough to consider diffusion of substitutional elements negligible, can be estimated at 10 to 15 hours, depending on the mass of the coil and the position considered.

An estimate of the carbon enrichment in austenite before the start of the low-temperature transformations can be attempted based on the microstructural analysis. It is assumed that the formation of ferrite produces a full partitioning of carbon, whereas bainite retains the carbon content of the parent phase and the partitioning of carbon occurs only after the bainitic ferrite units are formed, thus producing the precipitation of inter-lath carbides.

Considering that strips S1 and S2 contain 0.09 wt% carbon, strips S3 and S4 0.07 wt% carbon and that the average carbon content in ferrite is at a first approximation 0.020 wt%, by a simple mass balance it is estimated that, before the bainite starts, in strip S1 austenite has 0.14 wt% carbon and in S3 0.13 wt%. But since the cooling on the ROT is carried out down to a temperature below  $B_s$ , upper bainite can form and the transformation is expected to be finished before the strip is coiled.

In strips S2 and S4 ferrite forms on the ROT as well, but the phase transformation finish is expected to occur in the coiled strip with an austenite containing about 0.22 and 0.25 wt% carbon, respectively.

Looking for a possible explanation of the presence of martensite in strips S2 and S4 instead of bainite, the schematic calculated paraequilibrium phase diagram reported in Fig. 6 can be of help. The filled circles represent the position of the four specimens in terms of coiling temperature and estimated range of carbon in the enriched austenite (horizontal error bars) just

after the formation of ferrite. In equilibrium conditions cementite precipitation should occur along the extrapolated  $A_{cm}$  curve. The  $T_0$  line is the locus of points where ferrite and austenite with the same composition have equal molar Gibbs free energy. Any displacive transformation cannot occur at temperatures above this line. On the same graph also the curve of  $T_0'$  temperature is shown. This takes into consideration an additional energy contribution to the molar Gibbs free energy of 400 J/mol, thus representing the upper limit of bainite formation.

Points S2 and S4 (high coiling temperature), being located on the left-hand side of the  $A_{cm}$ , are expected not to precipitate any cementite. They are associated to a quite stable austenite, thanks to the additional effect of Mn, Mo and Cr, with a homogeneous level of carbon in its interior. Owing to the very slow cooling rate of the coil, a partial - if not complete - partitioning of substitutions is highly probable. This makes the ferrite transformation sluggish and, when bainite could start forming, it faces with an unexpectedly stable austenite matrix. Thus, it seems reasonable that in strips S2 and S4 the condition called “incomplete bainite reaction” is met. According to Bhadeshia and Edmonds [28, 29], the austenite highly enriched in carbon is so stable that the diffusionless transformation is thermodynamically impossible. Namely, the free energy of the residual austenite becomes less than that of the bainitic ferrite of the same composition. This condition is theoretically fulfilled along the  $T_0'$  curve.

As it can be observed in Fig. 6, both S2 and S4 strips are beyond the  $T_0'$  curve, at least when the strip is coiled, and no bainite transformation is expected to occur as the coil cools down, until the line of the actual  $M_s$  temperature of the enriched austenite is reached. In addition, if the systems tend towards a full partitioning of substitutions between ferrite and austenite, the  $T_0'$  curve shifts at even lower

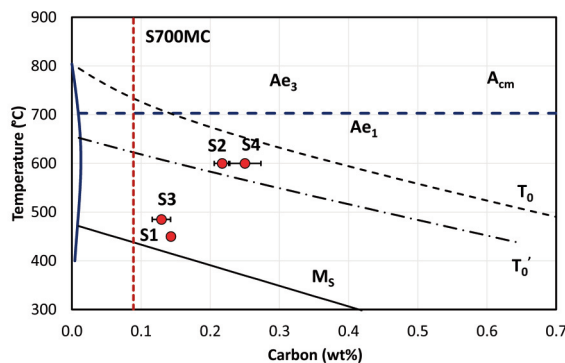


**Figure 6.** Schematic paraequilibrium phase diagram of the S700MC steel calculated with the average composition. The filled circles represent the position of the four specimens in terms of coiling temperature and estimated range of carbon in the enriched austenite (horizontal error bars)

temperatures compared to that estimated according to a paraequilibrium condition, further reinforcing the proposed mechanism.

From the viewpoint of the industrial production this aspect deserves a specific and more accurate investigation because it can represent an issue on the mechanical stability of the coiled strip. As a matter of fact, when the phase transformation reaches the completion after the strip has been coiled, the strip tension might relax, thus causing the ovalization of the coil.

As additional support to the hypothesis of incomplete bainite reaction, it is worth mentioning that the most promising recent theories on this phenomenon involve the cessation of growth induced by the coupled solute drag effect, accentuated by the overlap of carbon diffusion fields associated with nearby ferrite crystals, as discussed by Caballero and Bhadeshia [30] and also by Aaronson et al. [31]. Although these theories need further experimental support, nevertheless they depict a scenario very similar to that illustrated for strips S2 and S4. This phenomenon has been also observed by Ławrynowicz [32] in medium carbon steels alloyed with Mn, Mo, Cr, V, and Ti.

Summarizing, the transformation behaviour of the steels S3 and S4 coiled at 600°C, a temperature higher than that of the standard practice for this grade (450°C), appears similar despite the difference in thickness and the consequent difference in the cooling rate along the run-out table. At the same time this corroborates the proposed mechanism which instead relies on a phase transformation which achieves its completion after a long time at a relatively high temperature above the Bs.

#### 4.2. Analysis of the mechanical behaviour

The mechanical behaviour of the strips has been investigated in detail by calculating the parameters of the Hollomon analysis from the plot of  $\ln(\sigma)$  versus  $\ln(\epsilon)$  according to the relationship  $\sigma = K \cdot \epsilon^n$ . The numerical data are reported in Tab. 5. An excellent linear fit has been obtained in all cases in the true strain range 0.018-0.082 (i.e. from yielding to the onset of necking). The strain hardening coefficient  $n$  increases from S1 to S2 and it slightly decreases from S3 to S4, but it has to be taken into account that the

**Table 5.** Hollomon analysis of the stress-strain curves of the studied specimens

	S1	S2	S3	S4
$K$ (MPa)	6.99	7.28	7.10	7.15
$n$	0.0835	0.1186	0.1409	0.1260
correlation coefficient	0.999	0.996	0.999	1.000
$e$ at necking	0.0735	0.0810	0.0889	0.0957



stress-strain curve of S3 has a wider Lüders elongation segment that might introduce some bias. At the same time, the onset of necking, determined as the point where  $d\sigma/d\varepsilon = \sigma$ , shifts towards higher strains as the coiling temperature increases.

The increase in  $R_m$  from the low-T coiled to the high-T coiled strips can be explained invoking the higher strain hardening rate associated to the presence of martensite in S2 and S4. A further strengthening contribution due to precipitation of small particles is possible, as suggested by Kostryzhev and Marenych [33] and Oktay et al. [8] for similar steels after holding at 600°C.

This is apparent in Fig. 7 where the strain hardening rate  $d\sigma/d\varepsilon$  is plotted versus the true strain. The strain hardening rate decreases rapidly with increasing the strain during the initial stage of deformation and then decreases slowly. The strain hardening rate of the high-T coiled strips S2 and S4 is greater than that of S1 and S3 up to about a strain of 0.004. The curve of strip S1 is always below that of the corresponding S2 up to the onset of necking. Strip S3 has a different behaviour characterized by the lowest values at the very beginning, due to the presence of a more pronounced Lüders regime, followed by a sudden increase which leads the curve to superimpose those of S2 and S4, which are almost coincident in the final stages. This could be an effect of strain-induced transformation of the small austenite fraction (about 4 vol.%) observed by x-ray diffraction. The higher strain hardening rate of strips S2 and S4 at low strains is explained by the presence of hard martensite islands in a ferrite matrix, in analogy with DP steels, as observed by Tasan et al. [19]. Differences between homologous strips (S1-S3 and S2-S4) are mainly due to chemical composition and specifically to the carbon content.

Regarding the remarkable increase in the  $R_m$  of strips coiled at 600°C compared with those coiled at 450°C, a possible further contribution could be due to precipitation strengthening.

First of all, based on the steel chemical composition and considering that a coiling

temperature of 450°C is for sure too low to permit the precipitation of small NbC particles contributing to the matrix strengthening, it can be reasonably concluded that the coarse precipitation observed by SEM (80-250 nm) has been presumably formed during the hot rolling process.

Unfortunately, it has not been possible to carry out a characterization of the precipitation state by TEM to ascertain the presence of nanoprecipitation produced in ferrite during coiling at 600°C which is expected to be much finer than that previously mentioned and ranging from 2 to 40 nm in size. According to the literature, a coiling temperature of 600°C is actually a favourable condition to promote NbC precipitation in ferrite with a measurable strengthening contribution [34]

The reason why a parallel strengthening effect is not observed on the yield point of the strips coiled at high and low temperature is probably due to the transition from a continuous yielding to a discontinuous or quasi-continuous yielding, the former mode producing on average lower values than the latter one.

### 4.3. EBSD analysis

The area-weighted grain size distribution, the grain orientation spread (GOS) distribution, and the boundaries misorientation distribution determined by EBSD are here reported and discussed to provide a deeper insight into the microstructure of the studied strips.

The size distributions weighted on the grain area are shown in Fig. 8. These have been preferred to the numerical ones because they allow to better evaluate the presence of large grains and, in this respect, they reflect more closely as the microstructures appear after a visual examination. To this purpose, grains have defined and reconstructed from sets of neighbouring pixels having a misorientation less than 5 degrees between each other. It can be observed that in all strips the majority of grains are in the size range from 1 to 3  $\mu\text{m}$ . In strip S1 the distribution appears

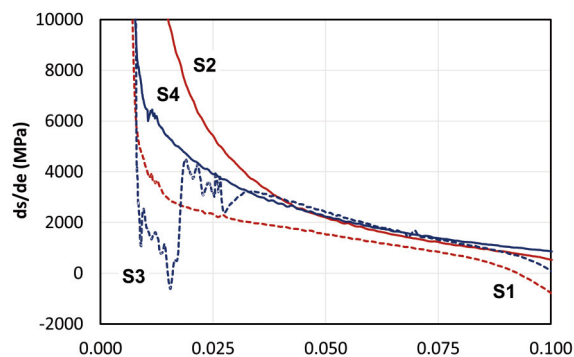


Figure 7. Calculated strain hardening rate of the studied S700MC strips

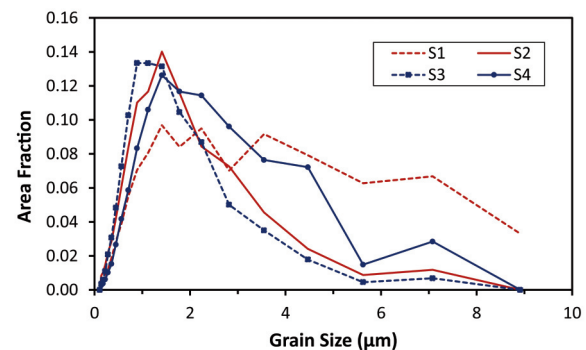
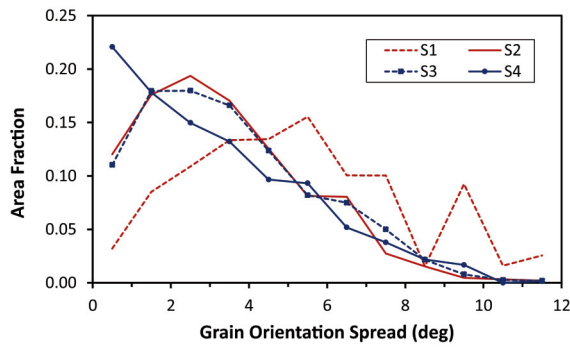


Figure 8. Distribution of area fraction as a function of grain size as determined by EBSD





**Figure 9.** Distribution of area fraction as a function of the grain orientation spread (GOS) determined by EBSD

bimodal since it is characterised by small grains of bainitic ferrite and by some larger regions with size from 4 up to 8  $\mu\text{m}$ . Their nature will be clarified later, when the GOS distributions are analysed. At the same time, as previously noticed in discussing the OM and SEM microstructures, the strip S4 exhibits a broader distribution compared to the other specimens, which

has been interpreted as the result of coarsening and of a lower overall deformation.

The GOS distributions are reported in Fig. 9. They suggest that, notwithstanding the different coiling temperature and thickness, strips S2 and S3 are very similar. Most of the microstructure appears to have a homogeneous orientation with a spread not greater than about 4 degrees. Then, the long tail towards higher misorientations is probably associated to acicular ferrite or bainitic ferrite. On the contrary, strip S1 shows the presence of regions with high internal misorientation spread, related to the larger grains evidenced in the Fig. 8. Finally, the strip S4 has a monotonously decreasing distribution of misorientations but most of the structure is concentrated at very low values, corresponding to ferritic grains with a low dislocation density and no substructure.

All the above features appear clearly in the GOS maps reported in Fig. 10 where the colour coding from blue to red identifies spreads in the range 0.2 to 15.5 degrees.

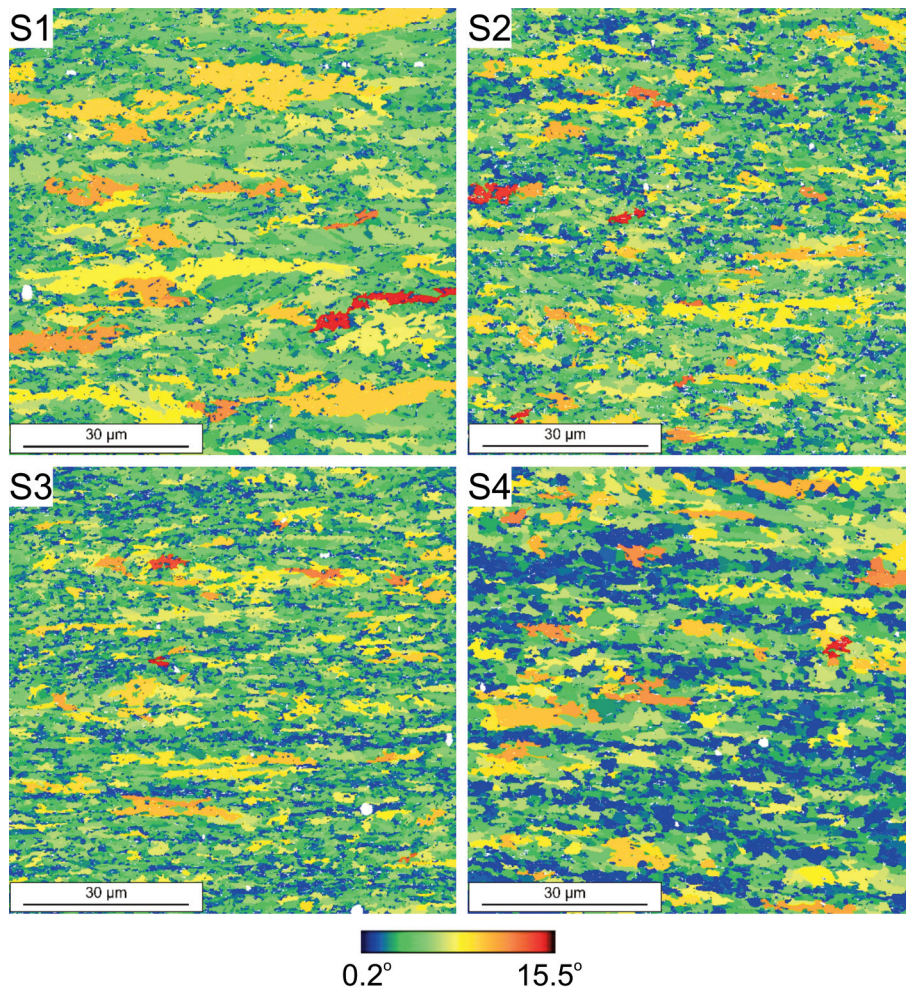


**Figure 10.** Grain orientation spread (GOS) maps determined by EBSD

The grain boundary misorientation distributions are shown in Fig. 11. At the same time, the mean size of sub-grains and packets has been measured by an automatic image analysis procedure on the EBSD grain boundary maps. These latter features are defined as the microstructural domains surrounded by boundaries with misorientation less or equal to  $5^\circ$  (low-angle grain boundaries, LAGBs) and higher or equal to  $15^\circ$  (high-angle grain boundaries, HAGBs), respectively following for example Di Schino and Guarnaschelli [35], Caballero et al. [36] and Javaheri et al. [37].

As it can be observed from Fig. 11, the strip S1 has the highest fraction of grain boundaries with a misorientation below  $15^\circ$ , which are associated to upper bainite according to Zajac et al. [38] and DeArdo et al. [39]. Although at a lesser extent, S3 also has a higher fraction of LAGBs compared to S4. This finding is in agreement with the smaller fraction of bainite estimated in Tab. 3 by optical metallography. At the same time, the strips S2 and S4 coiled at high temperature exhibit a higher characteristic peak at  $60^\circ$  associated to the presence of martensite.

According to Di Schino and Guarnaschelli [35], the structural unit controlling the yield strength is the sub-grain (delimited by LAGBs) acting as an effective barrier to dislocation movement. On the other hand, the critical cleavage stress and the impact energy are controlled by the covariant (bainitic or martensitic) packet delimited by HAGBs. The results of the automatic image on the EBSD maps have revealed no significant differences in the mean size of both these features among the specimens.

Therefore, the lower impact toughness of the high-temperature coiled strips S2 and S4 can be explained not only as due to the almost complete absence of bainite, a constituent known for having a better cracking resistance than ferrite, but principally to the presence of less resilient ferrite-martensite interfaces instead of a smaller packet size.

As a final remark, it is worth noticing that strips S2 and S4, although they do not contain bainite as one

of the major constituents, exhibit mechanical properties and a chemical composition somehow similar to that of the so-called “complex phase” steels. In fact, according to the EN10346-2015 standard, the CP800 grade in longitudinal direction should have  $R_{p0.2}$  from 660 to 830 MPa,  $R_m$  greater than 760 MPa and a total elongation greater than 10%, with a chemical composition (in mass) of  $C < 0.18\%$ ,  $Mn < 2.5\%$ ,  $Cr + Mo < 1\%$ ,  $Nb + Ti < 0.25\%$ .

Nevertheless, regarding a possible use of the present grade variant in automotive applications, the flangeability performance requires further investigations since the high fraction of martensite could represent an issue.

## 5. Conclusions

If the coiling temperature of 6 mm and 10 mm thin strips of a boron-free S700MC steel grade is increased from the usual low target value of about  $450^\circ\text{C}$  (below the bainite starting temperature) to  $600^\circ\text{C}$ , a ferrite-martensite structure is obtained instead of the expected ferrite-bainite microstructure. This change is reflected into a slight decrease of the yield point and a significant increase in ultimate tensile strength (not below 80 MPa), with a transition from a quasi-discontinuous to a clearly continuous yield behaviour. At the same time, the ratio of yield strength to tensile strength decreases from 0.90 to 0.75 and the impact energy from 35 J to 60 J.

The mechanical behaviour of the strips coiled at high temperature is a direct consequence of the two-phase structure with a hard phase interspersed in a soft ferrite matrix. In these strips, the reduction in impact energy is due to the altered distribution of grain boundary misorientation distribution, which is related, on the one hand to the almost complete absence of bainite, a constituent known to have a better crack resistance than ferrite, and, on the other hand to the presence of less resilient ferrite-martensite interfaces.

In order to explain the presence of martensite in

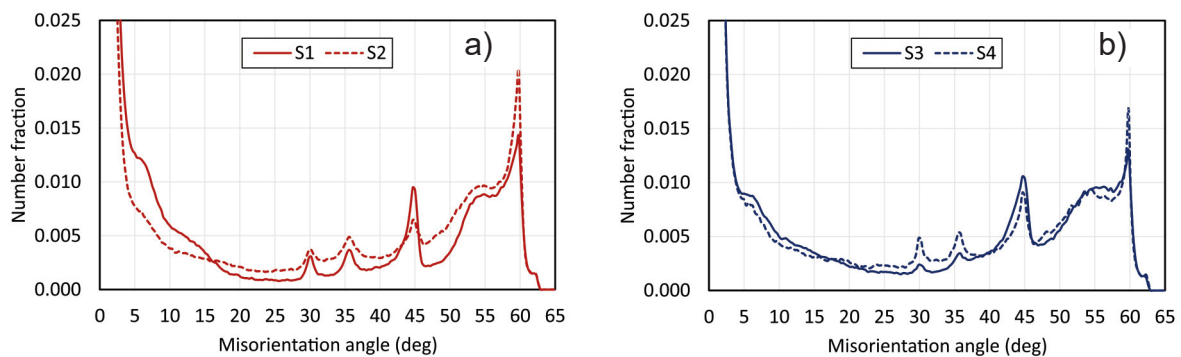


**Figure 11.** Grain boundary misorientation distribution of strips a) S1 and S2 (6 mm thickness) and b) S3 and S4 (10 mm thickness)

the final structure of the strips coiled above the Bs temperature it was hypothesized that the partial transformation into ferrite after coiling and the long time required for the cooling of the coil justify a significant stabilization of the not yet transformed austenite due to carbon enrichment as well as a possible further distribution of substitutional elements, making the bainite reaction impossible at lower temperatures.

However, since it was noticed that the austenite has not completely transformed when the strip is coiled, the risk of mechanical instability of the coil should be taken into account.

### Acknowledgements

*We are thankful to Mr. Alp Yalcin from Metal Forming Center of Excellence of Atilim University for his help with the EBSD measurements.*

### Authors' contributions

*S.O.: Conceptualization, Formal analysis, Investigation, Resources, Writing-review & editing, Supervision; P.E.D.N.: Conceptualization, Formal analysis, Writing-original draft, Writing-review & editing, Supervision; M.C.C.: Writing-review & editing, Supervision; K.D.: Investigation, Resources, Writing-review & editing; M.K.Ş.: Resources, Supervision.*

### Conflict of interest

*The authors declare no conflict of interest.*

### References

- [1] T. Usta, A. Çdçek, N. Uçak, V. Çeldk, S. Agca, Performance evaluation of S700MC and ST52 steels in terms of mechanical properties and fatigue life, Proc. Int. Conf. Metal 2016, Brno, Czech Republic, 2016, 549-554 25th International Conference On Metallurgy And Materials Metal 2016 ISSN: 2694-9296, ISBN: 978-80-87294-67-3. <https://www.confer.cz/metal/2016>.
- [2] C. Mesplont, T. Waterschoot, S. Vandeputte, D. Vanderschueren, B.C. De Cooman, Development of High-Strength Bainitic Steels for Automotive Applications, Proc. 41st Mechanical Working and Steel Processing conference proceedings, Baltimore, MD, vol. 37 (1999) p. 515-524.
- [3] J. Bian, H. Mohrbacher, J.-S. Zhang, Y.-T. Zhao, H.-Z. Lu, H. Dong, Application potential of high performance steels for weight reduction and efficiency increase in commercial vehicles, Advances in Manufacturing 3 (2015) 27–36. <https://doi.org/10.1007/s40436-015-0102-9>.
- [4] E. Vuorinen, N. Hosseini, A. Hedayati, E. Kornacker, M.T. Fernandez, J. Sanz, M.I. Gonzalez, E. Cañibano, Mechanical and microstructural evaluation of high performance steel (S700MC) for road restraint systems, Engineering Failure Analysis 108 (2020) 104251. <https://doi.org/10.1016/j.engfailanal.2019.104251>.
- [5] A. Lugovskaya, Z. Yanushkevich, M. Odnobokova, A. Belyakov, R. Kaibyshev, Effect of thermomechanical treatment on microstructure and mechanical properties of high-strength low-alloy steel, AIP Conference Proceedings, Tomsk, Russia, vol. 1909 (2017) 020120. <https://doi.org/10.1063/1.5013801>.
- [6] A. Dolzhenko, Z. Yanushkevich, S.A. Nikulin, A. Belyakov, R. Kaibyshev, Impact toughness of an S700MC-type steel: Tempforming vs ausforming, Materials Science & Engineering A 723 (2018) 259–268. <https://doi.org/10.1016/j.msea.2018.03.044>.
- [7] J. Górka, Changes in the structure and properties of the steel S700MC by heat treatment, Advanced Materials Research, 1036 (2014) 111-116. <https://doi.org/10.4028/www.scientific.net/AMR.1036.111>.
- [8] S. Oktay, P.E. Di Nunzio, M.K. Şeşen, Investigation of the effect of isothermal heat treatments on mechanical properties of thermo-mechanically rolled S700MC Steel Grade, Acta Metallurgica Slovaca 26 (2020) 11-16. <https://doi.org/10.36547/ams.26.1.449.11>.
- [9] S. Shakil, W. Lu, J. Puttonen, Experimental studies on mechanical properties of S700 MC steel at elevated temperatures, Fire Safety Journal 116 (2020) 103157. <https://doi.org/10.1016/j.firesaf.2020.103157>.
- [10] J. Górka, Microstructure and properties of the high-temperature (HAZ) of thermo-mechanically treated S700MC high-yield-strength steel, Materials and Technology, 50 (2016) 617-621. <https://doi.org/10.17222/mit.2015.123>.
- [11] B. Szczucka-Lasota, T. Węgrzyn, B. Łazarz, T. Szymczak, A. Jurek, K.I. Wilczyński, P. Cybulko, MAG welding process for S700MC steel, Proc. XIV International Conference On Metal Structures (Icms2021), Rutledge, Poznań, Poland, Modern Trends in Research on Steel, Aluminium and Composite Structures (Gizejowski et al Eds.), 2021, <https://doi.org/10.1201/9781003132134>.
- [12] J. Moravec, I. Novakova, J. Sobotka, H. Neumann, Determination of grain growth kinetics and assessment of welding effect on properties of S700MC steel in the HAZ of welded joints, Metals 9 (2019) 707. <https://doi.org/10.3390/met9060707>.
- [13] T. Kik, J. Moravec, M. Švec, Experiments and numerical simulations of the annealing temperature influence on the residual stresses level in S700MC steel welded elements, Materials 13 (2020) 5289. <https://doi.org/10.3390/ma13225289>.
- [14] H. Mohrbacher, M. Spöttl, J. Paegle, Innovative manufacturing technology enabling light weighting with steel in commercial vehicles, Advances in Manufacturing 3 (2015) 3–18. <https://doi.org/10.1007/s40436-015-0101-x>.
- [15] U. Gürol, S.C. Kurnaz, Effect of carbon and manganese content on the microstructure and mechanical properties of high manganese austenitic steel, Journal of Mining and Metallurgy Section B: Metallurgy 56 (2020) 171-182. <https://doi.org/10.2298/JMMB191111009G>.
- [16] H. Pouraliakbar, G. Khalaj, M.R. Jandaghi, Khalaj M.J., Study on the correlation of toughness with chemical composition and tensile test results in microalloyed API pipeline steels, Journal of Mining



- and Metallurgy Section B: Metallurgy 51 (2015) 173-178. <https://doi.org/10.2298/JMMB140525025P>
- [17] A. Grajcar, P. Skrzypczyk, R. Kuziak, K. Gołombek, Effect of finishing hot-working temperature on microstructure of thermomechanically processed Mn-Al multiphase steels, *Steel Research* 85 (2014) 1058-1069. <https://doi.org/10.1002/srin.201300227>.
- [18] M. Morawiec, A. Skowronek, M. Król, A. Grajcar, Dilatometric Analysis of the austenite decomposition in undeformed and deformed low-carbon structural steel, *Materials* 13 (2020) 5443. <https://doi.org/10.3390/ma13235443>.
- [19] C.C. Tasan, M. Diehl, D. Yan, M. Bechtold, F. Roters, L. Schemmann, C. Zheng, N. Peranio, D. Ponge, M. Koyama, K. Tsuzaki, D. Raabe, Overview of dual-phase steels: advances in microstructure-oriented processing and micromechanically guided design, *Annual Review of Materials Research* 45 (2015) 391-431. <https://doi.org/10.1146/annurev-matsci-070214-021103>.
- [20] A. Graux, S. Cazottes, D. De Castro, D. San-Martín, C. Capdevila, J.-M. Cabrera, S. Molas, S. Schreiber, D. Mirković, F. Danoix, D. Fabrègue, M. Perez, Design and development of complex phase steels with improved combination of strength and stretch-flangeability, *Metals* 10 (2020) 824. <https://doi.org/10.3390/met10060824>.
- [21] H.K.D.H. Bhadeshia, *Bainite in steels, transformations microstructure and properties*, second edition, IOM, London, 2001.
- [22] B. Josefsson, H.-O. Andrén, Microstructure of granular bainite, *Journal de Physique Colloques*, 49 (1988) C6/293-C6/298. <https://doi.org/10.1051/jphyscol:1988651>.
- [23] F. Boratto, R. Barbosa, S. Yue, J.J. Jonas, Effect of chemical composition on critical temperatures of microalloyed steels, *Proc. International Conference on Physical Metallurgy of Thermomechanical Processing of Steels and Other Metals. THERMEC-88*, Iron and Steel Institute of Japan, Tokyo, 1988, p. 383-390.
- [24] P.E. Di Nunzio, unpublished research, RC-CSM internal report, 2014.
- [25] E. Kozeschnik, *Modeling solid-state precipitation*, Momentum Press, 2013, ISBN 978-1-60650-062-0, (<https://www.matcalc.at/>). <https://doi.org/10.5643/9781606500644>.
- [26] R.C. Reed, H.K.D.H. Bhadeshia, Kinetics of reconstructive austenite to ferrite transformation in low alloy steels, *Materials Science and Technology* 8 (1992) 421-435. <https://doi.org/10.1179/mst.1992.8.5.421>.
- [27] D. Koistinen, R. Marburger, A general equation prescribing the extent of the austenite-martensite transformation in pure iron-carbon alloys and plain carbon steels, *Acta Metallurgica*, 7 (1959) 59-60. [https://doi.org/10.1016/0001-6160\(59\)90170-1](https://doi.org/10.1016/0001-6160(59)90170-1).
- [28] H.K.D.H. Bhadeshia, D.V. Edmonds, The bainite transformation in a silicon steel, *Metallurgical Transactions A*, 10A (1979) 895-907. <https://doi.org/10.1007/BF02658309>.
- [29] H.K.D.H. Bhadeshia, D.V. Edmonds, The mechanism of bainite formation in steels, *Acta Metallurgica* 28 (1980) 1265-1273. [https://doi.org/10.1016/0001-6160\(80\)90082-6](https://doi.org/10.1016/0001-6160(80)90082-6).
- [30] F.G. Caballero, H.K.D.H. Bhadeshia, Very strong bainite, *Current Opinion in Solid State and Materials Science*, 8 (2004) 251-257. <https://doi.org/10.1016/j.cossms.2004.09.005>.
- [31] H.I. Aaronson, W.T. Reynolds Jr, G.R. Purdy, The incomplete transformation phenomenon in steel, *Metallurgical and Materials Transactions A*, 37A (2006) 1731-1745. <https://doi.org/10.1007/s11661-006-0116-9>.
- [32] Z. Ławrynowicz, Bainite transformation in experimental Fe-Cr-Mo-V-Ti-C steel, *Advances in Materials Science*, 13 (2013) 12-18. <https://doi.org/10.2478/adms-2013-0005>.
- [33] A.G. Kostyryzhev, O.O. Marenych, Superior mechanical properties of microalloyed steels processed via a new technology based on austenite conditioning followed by warm deformation, *Materials Science and Engineering: A* 688 (2017) 16-19. <https://doi.org/10.1016/j.msea.2017.01.102>.
- [34] M.A. Altuna, A. Iza-Mendia, I. Gutiérrez, Precipitation of Nb in ferrite after austenite conditioning. Part II: Strengthening contribution in high-strength low-alloy (HSLA) steels, *Metallurgical and Materials Transactions A*, 43 (2012) 4571-4586. <https://doi.org/10.1007/s11661-012-1270-x>.
- [35] A. Di Schino, C. Guarnaschelli, Effect of microstructure on cleavage resistance of high-strength quenched and tempered steels, *Materials Letters*, 63 (2009) 1968-1972. <https://doi.org/10.1016/j.matlet.2009.06.032>.
- [36] F.G. Caballero, H. Roelofs, S. Hasler, C. Capdevila, J. Chao, J. Cornide, C. Garcia-Mateo, Influence of bainite morphology on impact toughness of continuously cooled cementite-free bainitic steels, *Materials Science and Technology*, 28 (2012) 95-102. <https://doi.org/10.1179/1743284710Y.0000000047>.
- [37] V. Javaheri, N. Khodaie, A. Kaijalainen, D. Porter, Effect of niobium and phase transformation temperature on the microstructure and texture of a novel 0.40% C thermomechanically processed steel, *Materials Characterization* 142 (2018) 295-308. <https://doi.org/10.1016/j.matchar.2018.05.056>.
- [38] S. Zajac, V. Schwinn, K.H. Tacke, Characterisation and quantification of complex Bainitic microstructures in high and ultra-high strength linepipe steels, *Materials Science Forum* 500-501 (2005) 387-394. <http://dx.doi.org/10.4028/www.scientific.net/MS>.
- [39] A.J. DeArdo, C. Cayron, L.P. Karjalainen, P.P. Suikkanen, Crystallographic analysis of martensite in 0.2C-2.0Mn-1.5Si-0.6Cr steel by EBSD, *La Metallurgia Italiana*, 9/2011, 13-22. [http://www.aimnet.it/allpdf/pdf\\_pubbli/set11/DEARD O.pdf](http://www.aimnet.it/allpdf/pdf_pubbli/set11/DEARD O.pdf).



## UTICAJ TEMPERATURE NAMOTAVANJA NA STRUKTURU I SVOJSTVA TERMO MEHANIČKI VALJANOG S700MC ČELIKA

S. Oktay <sup>a</sup>, P.E. Di Nunzio <sup>b\*</sup>, M.C. Cesile <sup>b</sup>, K. Davut <sup>c</sup>, M.K. Şeşen <sup>d</sup>

<sup>a</sup> Tehnički univerzitet u Istanbulu, Istanbul, Turska

<sup>b</sup> RINA konsalting–Centar za razvoj materijala S.p.A., Rim, Italija

<sup>c</sup> Odsek za nauku o materijalima i inženjerstvo, Institut za tehnologiju u Izmiru, İzmir, Turska

<sup>d</sup> Tehnički univerzitet u Istanbulu, Istanbul, Turska

### Apstrakt

Čelik S700MC bez bora se obično proizvodi korišćenjem svojstava mešane strukture ferit-bejnit formirane namotavanjem traka na temperaturi od oko 450°C, odnosno ispod početne temperature beinita. U cilju daljeg poboljšanja mehaničkih svojstava traka debljine od 6 do 10 mm, vršena su industrijska ispitivanja na temperaturi namotavanja od 600°C kako bi se podstaklo formiranje strukture ferita i karbida koja je takođe prihvatljiva za ovu vrstu čelika. Neočekivano je dobijena struktura ferita i martenzita. U poređenju sa feritno-beinitnom klasom, novu mikrostrukturu karakteriše blagi pad granice tečenja, ali povećanje zatezne čvrstoće za ne manje od 80 MPa, sa prelaskom sa kvazi-diskontinuiranog na jasno kontinuirano tečenje. Shodno tome, odnos granice razvlačenja i zatezne čvrstoće se smanjuje sa 0,90 na 0,75, a energija udara se smanjuje za 35 J i 60 J, pojedinačno, za dva nivoa debljine.

Mehaničko ponašanje traka namotanih na visokoj temperaturi objašnjava se kao direktna posledica dvofazne strukture sa tvrdom fazom u matrici mekog ferita. Prisustvo martenzita se objašnjava takozvanom nepotpunom beinitnom reakcijom. Delimična transformacija u ferit nakon namotavanja i dugo vreme potrebno da se kalem ohladi stabilizuju netransformisani austenit zbog obogaćivanja ugljenikom, čineći formiranje beinita na nižim temperaturama nemogućim.

**Ključne reči:** HSLA čelici; Fazna transformacija; Mikrostruktura; EBSD tehnika; Mehanička svojstva

